Analysis of the Interaction of Jets and Airfoils in Two Dimensions

C. A Shollenberger*
McDonnell Douglas Research Laboratories, St. Louis, Mo.

A solution for the flow of a jet in the proximity of one or more airfoils is developed to approximate the aircraft wing/engine interface. The two-dimensional, inviscid, incompressible case considered is a significant simplification of the real flow that has proved useful for similar problems. The jets and airfoils are represented by appropriate flow singularities. A general numerical formulation is developed to describe the airfoil and jet system that allows an iterative scheme to be constructed for determining the location and strength of the flow singularities. Example calculations, including jet shapes and aerodynamic characteristics, are presented for various configurations.

Nomenclature

A = actuator disk area
C = influence coefficient matrix
C_j = jet momentum coefficient
C_l = section lift coefficient
C_Q = jet mass flow coefficient
C_T = actuator thrust coefficient
c = length of airfoil chord
E = convergence parameter
F = force on airfoil
f = empirical entrainment function
H = total head of the flow
l = section lift
K = kernel function
M = airfoil pitching moment
N = number of wake segments
q = complex conjugate velocity
s = coordinate along a vortex sheet
T = actuator disk thrust
U = freestream flow speed
u = perturbation velocity in freestream direction
V = local flow speed
$\bar{V}$ = average flow speed
v = perturbation velocity perpendicular to freestream
x = coordinate parallel to freestream
y = coordinate perpendicular to freestream
z = complex coordinate $(x + iy)$
Γ = coefficient of vortex distributions
γ = strength of vortex sheet
θ = local flow angle relative to freestream
ν = iteration number
ρ = fluid density
ϕ = velocity potential
ω = relaxation parameter

Subscripts

a = airfoil
D = decaying vortex distributions
j = inside high-energy flow region
n = derivative with respect to normal coordinate
o = outside high-energy flow region
R = relaxation process
t = nose thrust
w = jet wake

Presented as Paper 72-777 at the AIAA 4th Aircraft Design, Flight Test, and Operations Meeting, Los Angeles, Calif., August 7-9, 1972; submitted August 31, 1972; revision received February 20, 1973. This research was conducted under the McDonnell Douglas Independent Research and Development Program.

Index categories: Airplane and Component Aerodynamics; Jets, Wakes, and Viscid-Inviscid Flow Interactions.

*Research Scientist, Flight Sciences Department. Member AIAA.

Introduction

NEARLY all powered flight involves some form of interaction between aircraft components and regions of high-energy flow resulting from the propulsion system. Common examples of this interaction are propeller slipstream/wing and jet engine exhaust/airframe interference. Despite the fact that virtually every powered aircraft is influenced by the wing/engine interface, conventional designs generally ignore or minimize these effects. However, current efforts are directed toward advantageous use of the propulsive/lift interaction for design of specialized aircraft. These applications emphasize the need for more adequate analysis of the interaction and motivate the present investigation of a jet in the proximity of a solid surface such as an airfoil.

As mentioned previously, numerous applications of the interaction exist but probably the most extreme examples are current V/STOL lift schemes such as the externally blown jet flap illustrated in Fig. 1. This application is designed to provide high lift through favorable wing/jet interaction without the mechanical complexity associated with other proposals. Other applications of the airfoil/jet interaction include the augmentor wing, the ducted fan, and the jet flap. The present analysis is not limited to any specific configuration since it considers an arbitrary arrangement of lifting surfaces in a nonuniform flowfield, i.e., a flowfield with a region of flow of higher energy than the freestream.

Several analytical investigations have treated the wing in a propeller slipstream problem. References 1–4 are representative of these studies which are largely various refinements of techniques and involve restrictive idealization of the flow. The boundary conditions are linearized for small jet perturbation velocities and are applied at mean locations in the flowfield. The results of these analyses are scattered, and experimental verification is somewhat limited.

A second class of wing/jet analysis is the jet flap analysis originated by Spence[5] which assumes zero jet thick-

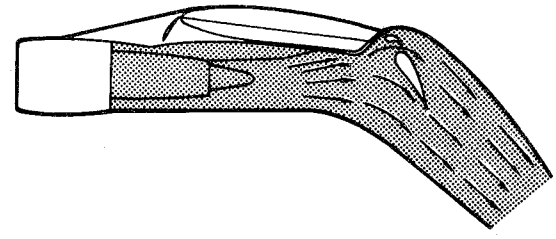

Fig. 1 Example of jet/airfoil interaction.

ness and zero mass flow but finite jet momentum. Solutions using this idealization and linearized for small jet deflection have shown remarkable agreement with experiments over a large range of jet angles. Jet flap analysis has been refined and extended to three dimensions and subsequently applied to systems where the assumptions of the analysis are clearly violated. Nevertheless, useful results have been obtained by this procedure, apparently resulting from fortuitous cancellation of errors caused by the violated conditions.

Analysis of a deflected, thick jet near an airfoil is developed in Ref. 6 by replacing the wing/jet system with a solid body of finite extent and numerically determining the flow about the resultant body. This method requires an assumption of jet shape and is limited to wing/jet systems that can be adequately represented by a single equivalent body.

In Ref. 7 a numerical method is presented to analyze a thick jet originating from between two lifting surfaces. No restrictions are imposed on jet energy or jet deflection. The following analysis is a generalization and extension of the procedure developed in Ref. 7. This analysis replaces the lifting surfaces and jet boundaries by their equivalent flow singularities embedded in a uniform stream. The exact boundary conditions are used to determine the strengths of the singularities and the location of the boundaries separating the regions of different total energy.

Analysis

Assumptions

The present analysis considers one or more airfoils in a flow which has a region of higher energy than the freestream. The primary assumptions are that the flow is inviscid, incompressible, and two-dimensional. Perfect fluid assumptions have yielded good results for jet flap analysis even though boundary layer and jet entrainment effects are ignored; thus, it is anticipated that these assumptions may be useful for the present problem. The two-dimensional flow condition simplifies the analysis significantly but may severely limit the use of the present method. Extensions of the analysis to approximate three-dimensional and viscous flows will be indicated later. Although high jet speeds may necessitate compressibility corrections, it appears that noise considerations will restrict many V/STOL lift systems to low jet speeds.

Boundary Conditions and Field Equations

The planar flow under investigation consists of two regions, an outer flow and a jet flow bounded on both sides by the outer flow as shown in Fig. 2. Since both regions are irrotational, a velocity potential exists for each region

$$\vec{V}_o = \nabla\phi_o \tag{1}$$

for the outer flow and, for the jet flow,

$$\vec{V}_j = \nabla\phi_j \tag{2}$$

Additionally, the flows are incompressible so that each velocity potential is Laplacian, or

$$\nabla^2\phi_o = 0 \tag{3}$$

and

$$\nabla^2\phi_j = 0 \tag{4}$$

The boundary condition on all solid surfaces is the usual inviscid condition of zero normal flow through the boundary, or

$$\phi_{o_n} = 0 \tag{5}$$

on all surfaces.

Jet boundary conditions are more complex since they include a pressure condition. The Bernoulli equation applied at the jet boundary gives

$$1/2\rho V_o^2 + \Delta H = 1/2\rho V_j^2 \tag{6}$$

where ΔH is the total pressure difference between the two regions which was added to the high-energy flow at an ideal fan or actuator disk. Here also V_o and V_j are the flow speeds outside and inside the jet boundary, respectively. Simple rearrangement of Eq. (6) yields

$$V_j - V_o = \Delta H/\rho\bar{V} \tag{7}$$

where $\bar{V}$ is the average flow speed at the jet boundary. The jet boundary is, therefore, a line where a discontinuity of velocity occurs which is related to the total pressure difference between the jet and freestream.

A second condition on the jet boundary prevents flow through the boundary,

$$\phi_{j_n} = 0 \tag{8}$$

It should be observed that, although Eqs. (7) and (8) are boundary conditions for the jet, the points of application of these conditions (the location of the jet boundaries) are unknown. Indeed, the unknown jet shape is a major difficulty in obtaining solutions for multienergy flows.

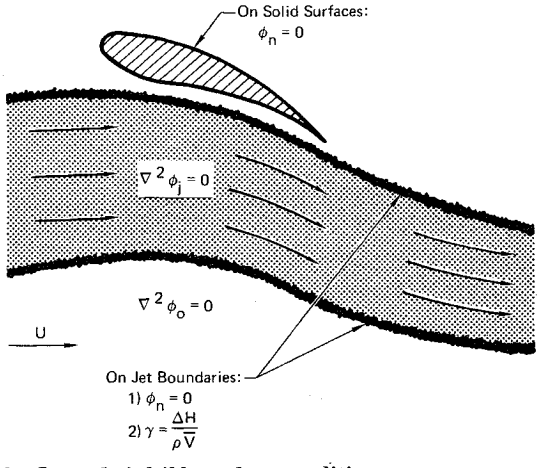

Fig. 2 Jet and airfoil boundary conditions.

Method of Solution

A numerical procedure to apply the foregoing boundary conditions will now be described to determine the jet and outer flowfields. The first step in this analysis is replacement of the various components of the problem by appropriate flow singularities. Several numerical methods have been developed using embedded singularities for solution of potential flow about solid surfaces. Presently flat plate airfoils will be considered, and consequently the appropriate singularity is a vortex sheet located along the chord of the airfoil. The strength of the vortex sheet will be determined by the solution procedure. Other airfoil shapes will be considered later.

The conditions of Eqs. (7) and (8) show that the jet boundaries are surfaces where the tangential velocity is discontinuous, indicating that the jet boundaries can be represented by vortex sheets whose strengths are related to the local mean velocity by Eq. (7). A method of solution must determine the strengths of the singularities and the location of the jet to determine the flow completely.

A set of simultaneous integral equations can be written to specify the airfoil/jet system. By use of the Biot-Savart

law, the velocity induced at (ξ,η) in the freestream direction by a vortex distribution, $\gamma(s)$, located between s_1 and s_2 on $x = x(s)$ and $y = y(s)$ is

$$u = \int_{s_1}^{s_2} \gamma(s) K_x(\xi, \eta, s) ds \tag{9}$$

Similarly, the velocity induced perpendicular to the freestream is

$$v = \int_{s_1}^{s_2} \gamma(s) K_y(\xi, \eta, s) ds \tag{10}$$

where the kernel functions K_x and K_y are functions of the geometry only. Now Eq. (5) can be written as

$$\int \gamma K_y ds = \tan\theta_a (U + \int \gamma K_x ds) \tag{11}$$

where θ_a is the surface angle of the airfoil and the integration is over the entire vortex systems of the airfoils and jet boundaries. Similarly, Eq. (7) can be written

$$\gamma_j [(\int \gamma K_y ds)^2 + (U + \int \gamma K_x ds)^2]^{1/2} = \frac{\Delta H}{\rho} \tag{12}$$

where γ_j is the strength of the jet boundary vorticity. Finally Eq. (8) gives

$$\int \gamma K_y ds = \tan\theta_j (U + \int \gamma K_x ds) \tag{13}$$

where θ_j is the local jet boundary angle.

To facilitate a numerical scheme of solution of these three integral equations, a general representation is required to describe all components of the system in terms of singularities embedded in a uniform stream. The flat plate airfoils can be simply represented by a vortex distribution along the chord line of the airfoil. In general there is a flow around the sharp leading edge of the plate, and hence there is an infinite velocity at this point which leads to the well-known square root singularity

$$\gamma \propto 1/(x)^{1/2} \tag{14}$$

where x is the distance from the leading edge. A combination of two basic vortex distributions adequately describes

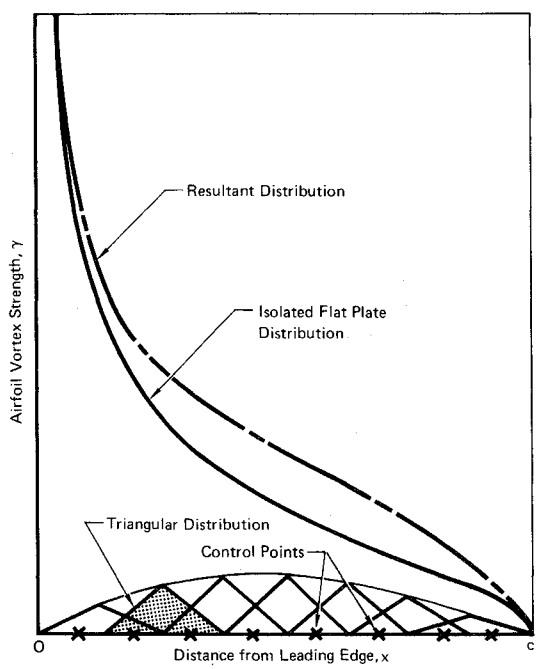

Fig. 3 Airfoil vortex distribution.

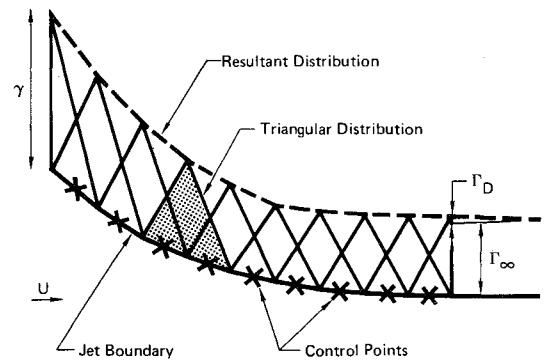

Fig. 4 Jet vortex distribution.

the flat plate. First the isolated flat plate distribution

$$\gamma_o = \Gamma_o [(c-x)/x]^{1/2} \tag{15}$$

provides the correct leading-edge behavior and is the correct limit for distant or weak jets. To allow perturbation from the loading of Eq. (15), a series of triangular vortex distributions are superimposed on the airfoil chord as shown in Fig. 3. The vortex strengths for the distributions are

$$\gamma_i = \Gamma_i \left(\frac{x_i - x}{x_i - x_{i-1}}\right) \text{ for } x_i \leqslant x \leqslant x_{i-1} \tag{16a}$$

$$\gamma_i = \Gamma_i \left(\frac{x_{i+1} - x}{x_{i+1} - x_i}\right) \text{ for } x_i \leqslant x \leqslant x_{i+1}, \text{ and} \tag{16b}$$

$$\gamma_i = 0 \text{ for } x \geqslant x_{i+1} \text{ or } x \leqslant x_{i-1} \tag{16c}$$

The combination of γ_o and several γ_i distributions provides the general formulation required for the airfoils and for the application of the Kutta condition at each airfoil trailing edge.

The triangular distributions of Eq. (16) are the basis of the jet boundary representation shown in Fig. 4. For the case of the jet, vorticity is placed on straight-line segments in the flow. The location of the vortex distribution, as well as values of Γ_i for the jet, will be determined by an iterative scheme. Two additional distributions are required to completely describe the jet far downstream of the airfoils.

For a two-dimensional jet which is deflected relative to freestream flow, the downstream jet direction must asymptotically approach the direction of the uniform onset flow. Violation of this condition results in an infinite force on the jet deflection system by application of the momentum theorem since a jet which continues to move downward at a finite rate would produce an infinite momentum flux in the vertical direction. As a consequence, the far downstream jet boundary can be represented by straight lines parallel to the freestream. The strength of the vortex sheet far downstream can be determined from Eq. (6) since $V_o = U$ at this position and hence

$$\frac{\Gamma_\infty}{U} = \left(\frac{\Delta H}{\rho U^2/2} + 1\right)^{1/2} - 1 \tag{17}$$

Using this value for Γ_∞, the jet boundary far downstream can be accurately represented by a constant vortex distribution on lines parallel to the freestream and extending to downstream infinity. To account for any mismatch between the strength of the last triangular vortex distribution Γ_N and Γ_∞, a decaying vorticity function also is incorporated into the wake representation.

$$\gamma_D = [(\Gamma_N - \Gamma_\infty)/x] x_N \text{ for } x > x_N \tag{18}$$

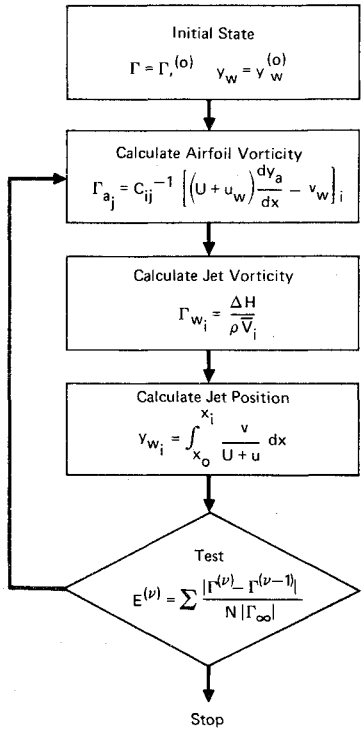

Fig. 5 Numerical procedure.

Now that the entire airfoil/jet system has been replaced by a general formulation of flow singularities, a procedure is required to determine the strength of the singularities and the jet location from application of the appropriate boundary conditions at numerous control points on the airfoil surface and along the jet boundaries. As indicated in Figs. 3 and 4, the control points selected will be at the midpoints between the triangular vortex distribution endpoints. The number of control points is equal to the number of triangular distributions on the airfoil and jet boundaries. An iterative technique is employed to determine the solution by alternatively solving for the airfoil and jet singularities. This process is illustrated by the flow chart in Fig. 5.

The first step of the iterative method is solution for the airfoil vortex distribution, assuming that the jet position and vorticity are known. The kinematic condition of no flow normal to the airfoil surface [Eq. (5)] can be expressed as

$$v/(U + u) = dy_a/dx \tag{19}$$

where $y_a(x)$ is the ordinate of the airfoil surface. The perturbations in the uniform flow u and v arise from two sources. First u_a and v_a result from the influence of the airfoils, and secondly u_w and v_w are induced by the jet. Hence Eq. (19) may be written

$$v_a - u_a\frac{dy_a}{dx} = (U + u_w)\frac{dy_a}{dx} - v_w \tag{20}$$

The right side of Eq. (20) can be determined at each airfoil control point from the assumed jet state by

$$q(z_p) = \frac{i}{2\pi}\int_{s_1}^{s_2}\frac{\gamma(s)}{z_p - z(s)}ds \tag{21}$$

where q is the complex conjugate velocity induced at z_p by a vortex distribution $\gamma(s)$ located between s_1 and s_2. The left side of Eq. (20) can be expressed as a matrix of influence coefficients C_{ij} multiplied by the airfoil vortex distribution coefficients.

$$v_{a_i} - (dy_a/dx)_i u_{a_i} = C_{ij}\Gamma_{aj} \tag{22}$$

The influence coefficient matrix is determined from the airfoil geometry by Eq. (21) and is used to form a set of linear equations for the present iteration's value of the airfoil vorticity

$$C_{ij}\Gamma_{a_j}^{(\nu)} = (U + u_{w_i}^{(\nu-1)})\left(\frac{dy_a}{dx}\right)_i - v_{w_i}^{(\nu-1)} \tag{23}$$

where the superscript denotes the iteration number.

With the values of Γ_a found from Eq. (23) a new wake state is determined. The dynamic boundary condition of Eq. (7) gives the local vortex strength at the ith control point as

$$\Gamma_{w_i}^{(\nu)} = \Delta H/\rho\bar{V}_i^{(\nu-1)} \tag{24}$$

Again the local velocity is calculated from the airfoil and jet vortex distributions using Eq. (21). By application of the kinematic jet boundary condition of Eq. (8), a new wake boundary position is calculated as

$$y_w^{(\nu)}(x) = y_o + \int_{x_o}^{x}\frac{v^{(\nu-1)}(x')}{U + u^{(\nu-1)}(x')}dx' \tag{25}$$

or, since the boundary is represented by straight line segments,

$$y_{w_i}^{(\nu)} = y_o + \sum_{j=1}^{i}\frac{v_j^{(\nu-1)}}{U + u_j^{(\nu-1)}}(x_j - x_{j-1}) \tag{26}$$

Repeated application of Eqs. (23, 24, and 26) forms the basis of the iterative scheme. To start the procedure, an initial ($\nu = 0$) jet position and vorticity is required. Additional required input is the airfoil coordinates, a step size for jet boundary elements, and the total pressure difference between the jet and freestream. Convergence of the process to a state where the boundary conditions are closely satisfied at all control points is tested by comparison of the vortex distributions of two successive iterations with the convergence parameter

$$E^{(\nu)} = \sum_{i=1}^{N}\frac{|\Gamma_{w_i}^{(\nu)} - \Gamma_{w_i}^{(\nu-1)}|}{N|\Gamma_\infty|} \tag{27}$$

When this parameter decreases to a specified small value, the iterative process is discontinued.

Numerous factors influence the rate of convergence of the iterative scheme, but the initial wake condition is the most important consideration. A useful initial wake shape is the streamline passing through the point where the jet originates. A useful jet vortex distribution to start the iterative scheme is a constant vortex strength of Γ_∞. Other factors influencing the convergence rate are the total pressure difference, angle-of-attack of the airfoils, and the proximity of airfoils and jet boundaries.

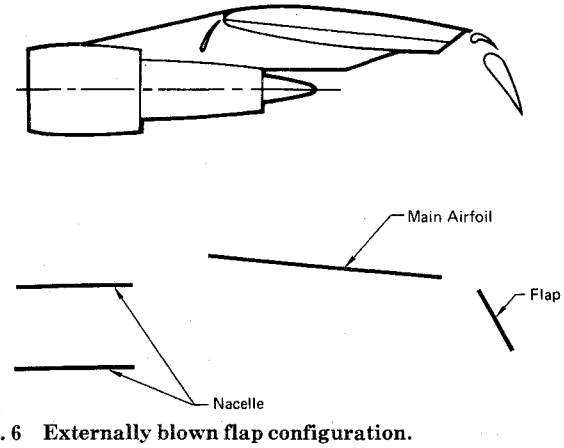

Fig. 6 Externally blown flap configuration.

A special feature to prevent the jet from flowing through an airfoil surface is included in the analysis to avoid this physically impossible condition. Flow through a surface could result from nonuniformly satisfying the boundary conditions only at a finite number of control points rather than at all points along the airfoil. The control feature checks each wake element to restrict it from violating the surface flow condition and adjusts the element slope if necessary. However, by careful choice of airfoil and jet element sizes, the check feature is necessary only for complex jet shapes.

Relaxation of the method by mixing the vorticity values of successive iterations to obtain a value for continuing the scheme is useful in improving the convergence rate. Using relaxation

$$\Gamma_{R_i}^{(\nu)} = \omega\Gamma_i^{(\nu)} + (1-\omega)\Gamma_i^{(\nu-1)} \tag{28}$$

Values of ω of about 0.5 (under relaxation) have improved convergence significantly.

After the iterative process has been terminated and a solution has been obtained, the forces and moments acting on the airfoils of the system can be determined. Forces are found by numerical integration of the Kutta-Joukowski law

$$F = \rho \int_o^c \gamma_a(x)\bar{V}(x)dx \tag{29}$$

The direction of this force is normal to the flat plate surface. A nose thrust force also is calculated that results from the infinite velocity around the leading edge yielding a force

$$F_t = (\rho\pi c/4)\Gamma_o^2 \tag{30}$$

where Γ_o is the coefficient of Eq. (15). This force acts parallel to the flat plate surface. Similarly, the pitching moments of the airfoils are determined by numerical integration

$$M = \rho \int_o^c x\gamma_a(x)\bar{V}(x)dx \tag{31}$$

for each surface.

Extension of the Present Method

Some of the assumptions of the analysis were incorporated to simplify the procedure while other restrictions resulted from basic limitations of the method of solution. For example, inclusion of thick and cambered airfoils is a simple extension of the foregoing development, but the three-dimensional or viscous problems require significant modification to the method and further approximation. Each of these cases will be considered in detail.

Limiting the airfoils to flat plates was a convenience since such airfoils can be simply represented as already described. More general airfoil sections can be analyzed by providing the appropriate flow singularities. For example, a flat plate with a flap requires a vortex distribution at the knee of the flap with an exponential form. Still more general airfoils can be analyzed by including provisions for thick sections. Source and sink distributions such as those used in Ref. 8 would be adequate, but the vortex singularities employed in Ref. 9 are more suitable for the present method since fewer control points are required for each airfoil. It is imperative to minimize the number of airfoil control points since the iterative nature of the method requires repeated solution of Eq. (23). With the flow singularities modified to include general airfoils, the remainder of the numerical procedure is applicable exactly as before.

Extension of the present method to three dimensions involves three difficulties: 1) the wake vorticity is of unknown direction; 2) the wake deforms in the crossflow plane; and 3) the downstream behavior is not direçtly determined. Each of these problems can be approximately resolved. Unlike the two-dimensional case where the direction of the jet vorticity is into the plane, the direction of the jet vorticity in three dimensions must be determined. However, the jet vorticity can be resolved into components parallel and perpendicular to the local mean velocity. The component perpendicular to the local flow is coupled to the total pressure difference and can be calculated from a dynamic condition similar to Eq. (7). The parallel component is determined by the change in the strength of the perpendicular component around the jet circumference. Three-dimensional wake deformation can be handled in a manner analogous to the two-dimensional case but involves greater complexity to apply the kinematic boundary condition of Eq. (8) to calculate the jet shape. The far downstream behavior of the three-dimensional jet is unknown but may be approximated by extension of the most distant downstream calculated shape and vorticity values. Accepted methods for representing wings, such as the vortex lattice method, can be combined with the three-dimensional jet model to complete the analysis. A final difficulty is the large number of elements required to describe the three-dimensional system adequately. This problem may be alleviated by the use of discrete vortex elements for the jet so that the computing time does not become prohibitive.

Viscous effects are expected to be confined to two aspects of the jet/airfoil interaction. The first is the influence of the boundary layer of the airfoil surfaces, which can be treated in a manner similar to ordinary airfoils. This includes calculation of the displacement thickness of the boundary layers from the pressure distributions obtained from the inviscid solution. The displacement thickness then is used to determine a new effective shape for the inviscid calculation. This process is repeated until the pressure distribution shows little change between successive calculating steps.

The second viscous effect significant in the jet/airfoil interaction is entrainment of the outer flow by the jet. Entrainment is completely ignored by the inviscid analysis but can be approximated by altering the kinematic wake condition of Eq. (8) to

$$\phi_{j_n} = f(x) \tag{32}$$

Then the wake boundary is determined by

$$y_w = y_o + \int_{x_o}^{x_i} \frac{v(x') + f(x')\cos\theta_j}{U + u(x') - f(x')\sin\theta_j}dx' \tag{33}$$

where $f(x)$ is determined from empirical results. Since the energy difference between the jet and freestream decreases downstream as more fluid is entrained by the jet, the total pressure difference must be scaled accordingly. Equation (33) for including entrainment is an approximation but provides a means for evaluating the importance of viscosity in the jet/airfoil interaction.

Discussion of Results

To illustrate the type of problems which can be analyzed by the foregoing method, consider the configuration of Fig. 6 which is the externally blown flap system of Ref. 10. The upper part of Fig. 6 is a cross section of one station of the wing tested in Ref. 10, and the lower part of the figure shows the system of flat plates used in the present calculations. The flat plate system, typical of externally blown jet flap configurations, consists of flap and airfoil elements with two nacelle airfoils from which a high-energy jet originates. Under the present analysis, a total pressure increase is made to the flow passing through

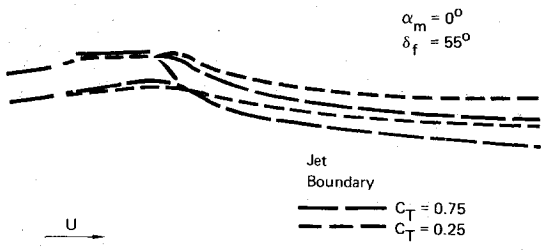

Fig. 7 Jet shape.

the nacelle airfoils. The flap chord is 0.31 of the main airfoil chord, and the nacelles are at an angle of 5.7° with the main airfoil. Ten control points were used on each airfoil of the system, and thirty-five wake elements were used on each of the two jet boundaries. The airfoil elements were of equal length, but the jet elements ranged from 0.4 to 0.05 of the combined airfoil-flap chord length. Large wake elements were sufficient far downstream, whereas small elements were necessary near the leading edge of the flap.

The jet boundary was represented by straight-line segments for five chord lengths downstream of the leading edge of the main airfoil and then by parallel lines of constant vorticity to downstream infinity. A starting solution for the jet shape was obtained by determining the streamlines originating from the trailing edges of the nacelle airfoils (at zero energy addition to the jet). A constant value of wake vortex strength was used for the initial iteration. Computation times for this system were about 0.05 min of IBM System/370 Model 195 central processor unit time per iteration. Usually seven iterations provide a convergence parameter value of $E^{(\nu)} = 0.00005$.

Figures 7 and 8 show the results of calculations at various engine thrusts and flap positions. The thrust coefficient C_T is the actuator disk thrust nondimensionalized by the disk area and freestream dynamic pressure

$$C_T = \frac{T}{(\rho U^2 A)/2} \tag{34}$$

Jet shapes of Fig. 7 are typical of the calculations with increasing thrust values resulting in greater jet deflections and jet contractions. The upper jet boundary is positioned

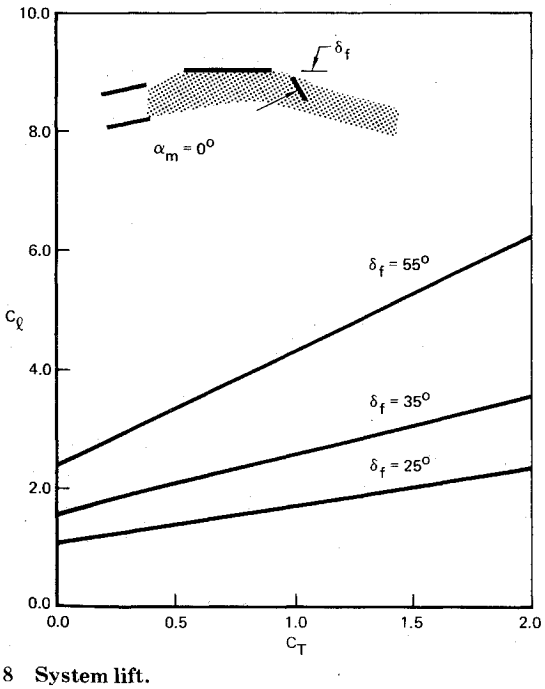

Fig. 8 System lift.

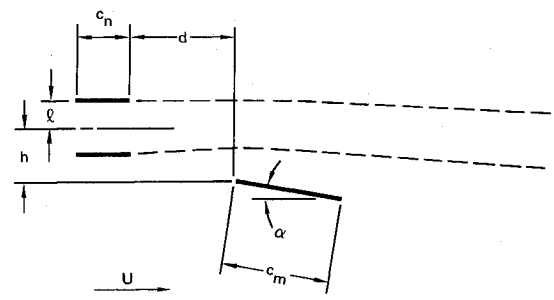

Fig. 9 Jet/airfoil system.

close to the main airfoil, but this has not introduced any major difficulty.

The lift curves of Fig. 8 show the variation of system lift with engine thrust. The system lift includes the lift on all airfoils and is nondimensionalized by the combined main airfoil-flap chord and the freestream dynamic pressure

$$C_l = \frac{l}{(\rho U^2 c)/2} \tag{35}$$

The largest part of the lift results from the force on the flap element which is immersed in the jet, but the main airfoil carries significant lift even though it is at zero angle-of-attack. The jet and flap induce a flow to cause the main airfoil to carry a substantial load. Forces on the engine nacelle airfoils are small compared with the total system lift for the current case. Note that, although Fig. 8 shows the system performance for variations of only two parameters C_T and δ_f, the procedure employed is capable of analyzing the effect of any of the numerous parameters of these configurations.

A second example, in Fig. 9, illustrates the influence of another parameter, the vertical location of a jet relative to an airfoil. Here a single airfoil interacts with a two-dimensional ducted fan system positioned upstream of the airfoil. All geometric parameters except the vertical position of the jet are constant for this example. The system lift is given in Fig. 10 for three values of jet energy. The system lift coefficient is the sum of all lift forces nondimensionalized by the main airfoil chord and the freestream dynamic pressure. The lift varies with h/c even for zero jet energy addition ($C_T = 0$) since the three airfoils

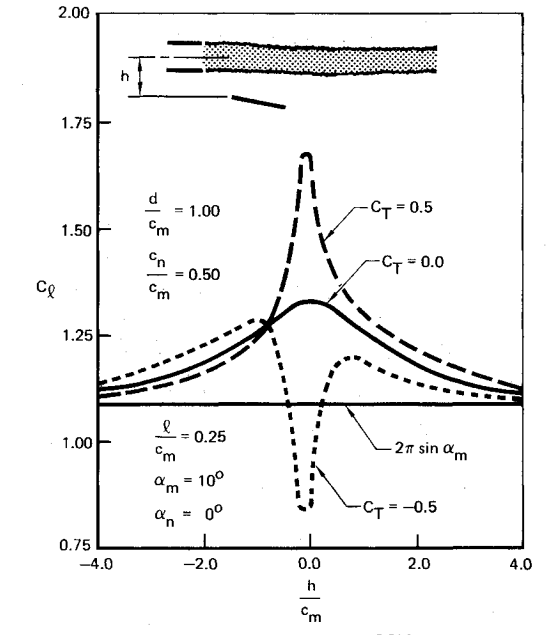

Fig. 10 Influence of jet position on airfoil lift.

interact. However, for the two values of nonzero jet energy difference shown in Fig. 10, the lift behavior is relatively complex. Lift for all values of C_T approaches the value of $2\pi \sin\alpha$ as $h/c \to \pm\infty$. Note that the case $C_T = -0.5$ corresponds to a jet of lower energy than the freestream and could result from the wake of a drag-producing body such as a radiator or windmilling fan between the nacelle airfoils. Also observe that a high-energy jet can result in lower system lift than the $C_T = 0$ case and that the low-energy wake can result in lift augmentation for certain positions of the jet. This example illustrates the possible complexity of system performance even for simple configurations.

A final example consisting of a two-dimensional ducted fan is shown in Fig. 11. In this configuration energy is added to the flow passing between two parallel flat plate airfoils of equal length. The calculated results of Fig. 11 show the system lift as a function of the jet mass flow for four values of jet momentum. The mass flow coefficient is defined as

$$C_Q = \rho_j V_j \delta / \rho U c \tag{36}$$

and the jet momentum coefficient is

$$C_j = \frac{(\rho_j V_j^2 \delta)}{(\rho U^2 c)/2} \tag{37}$$

where δ is the jet width. As C_Q approaches zero for a fixed C_j, the jet velocity increases and the jet thickness decreases. The jet flap formulation of Ref. 5 considers the limit of finite C_j for $C_Q \to 0$. This limit requires infinite jet velocity and zero jet thickness and therefore is difficult to calculate by the present method. Figure 11, however, shows the lift curve for decreasing C_Q with a linear extrapolation of the calculated results to $C_Q = 0$. These extrapolated values are in agreement with the jet flap results of Ref. 5 which also are indicated in Fig. 11. The jet vorticity associated with the jet flap formulation of Ref. 5 is the difference of the strengths of the jet vortex sheets of the present analysis.

Ideally the validity of the present solution method could be checked by comparison with experiments, but no two-dimensional experiments are available for the present configurations. Reference 7 shows agreement with experiment for two-dimensional ducted fan arrangements. However, further comparison is required to determine the usefulness of the present analysis.

Conclusions

A solution method for multienergy, inviscid, and incompressible flow in two dimensions for analyzing the interaction of jets and airfoils has been presented. The method is designed to aid in evaluation of multielement high lift airfoils which interact with propulsion systems. No linearizations were required to obtain the solution, and the only approximations are attributable to the numerical method. Calculations presented indicate the performance of some simplified high lift systems. Solutions readily provide the influences on the lift systems of the numerous parameters which are typical of these configurations. Guidance in optimizing these system parameters is an important goal of the present work, but additional experimental validation of the calculations is required before such application is justified.

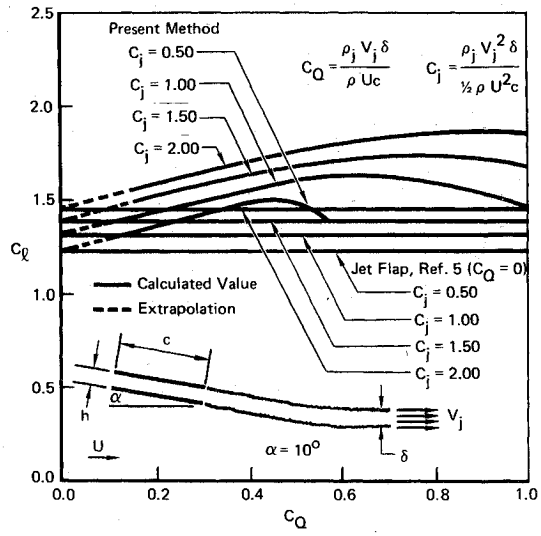

Fig. 11 Comparison with jet flap.

References

[1]Koning, C., "Influence of the Propeller on Other Parts of the Airplane," *Aerodynamic Theory*, Vol. IV, Springer-Verlag, Berlin, 1935.

[2]Graham, E. W., Lagerstrom, P. A., Licher, R. M., and Beane, B. J., "A Preliminary Theoretical Investigation of the Effects of Propeller Slipstream on Wing Lift," Rept. SM-14991, 1953, Douglas Aircraft Co., Long Beach, Calif.

[3]Rethorst, S. C., "Aerodynamics of Nonuniform Flows as Related to an Airfoil Extending Through a Circular Jet," *Journal of the Aeronautical Sciences*, Vol. 25, No. 1, 1958, pp. 11–28.

[4]Ribner, H. S. and Ellis, N. D., "Aerodynamics of Wing-Slipstream Interaction," *CASI Transactions*, Vol. 5, No. 2, 1972, pp. 56–63.

[5]Spence, D. A., "The Lift Coefficient of a Thin, Jet-Flapped Wing," *Proceedings of the Royal Society*, Ser. A, Vol. 238, 1956, pp. 46–68.

[6]Albers, J. A. and Potter, M. C., "Potential Flow Solution for a STOL Wing Propulsion System," TN D-6394, 1971, NASA.

[7]Shollenberger, C. A., "Analysis of a Two-Dimensional Propulsive-Lift System," CR-114457, 1972, NASA.

[8]Hess, J. L. and Smith, A. M. O., "Calculation of Potential Flow About Arbitrary Bodies," *Progress in Aeronautical Sciences*, Vol. 8, Pergamon Press, New York, 1966.

[9]Davenport, F. J., "Singularity Solutions to General Potential Flow Airfoil Problems," Rept. D6-7202, 1963, The Boeing Co., Seattle, Wash.

[10]Parlett, L. P., Fink, M. P., and Freeman, D. C., Jr., "Wind-Tunnel Investigation of a Large Jet Transport Model Equipped with an External-Flow Jet Flap," TN D-4928, 1968, NASA.